ACS Catalysis

Research Article

Cite This: ACS Catal. 2019, 9, 117−129

pubs.acs.org/acscatalysis

Site Activity and Population Engineering of NiRu-Layered Double Hydroxide Nanosheets Decorated with Silver Nanoparticles for Oxygen Evolution and Reduction Reactions

Soressa Abera Chala,[†] Meng-Che Tsai,[†] Wei-Nien Su,*[,‡] Kassa Belay Ibrahim,[‡] Alemayehu Dubale Duma,[‡] Min-Hsin Yeh,[†] Cheng-Yen Wen,[§] Chia-Hao Yu,[§] Ting-Shan Chan,[⊥] Hongjie Dai,*[,∥] and Bing-Joe Hwang*[,†,⊥]

[†]NanoElectrochemistry Laboratory, Department of Chemical Engineering, National Taiwan University of Science and Technology, Taipei 106, Taiwan

[‡]NanoElectrochemistry Laboratory, Department of Applied Science and Technology, National Taiwan University of Science and Technology, Taipei 106, Taiwan

[§]Department of Material Science and Engineering, National Taiwan University, Taipei 106, Taiwan

[∥]Department of Chemistry, Stanford University, Stanford, California 94305, United States

[⊥]National Synchrotron Radiation Research Center, Hsin-Chu 30076, Taiwan

Supporting Information

ABSTRACT: Developing efficient and durable bifunctional electrocatalysts for oxygen reduction and evolution reaction (ORR/OER) is highly desirable in energy conversion and storage systems. This study prepares nickel−ruthenium layered double hydroxide (NiRu-LDHs) nanosheets subjected to decoration with conductive silver nanoparticles (Ag NP/NiRu-LDHs), which interestingly induce their multivacancies associated with catalytic site activity and populations. The as-prepared Ag NP/NiRu-LDH shows excellent catalytic activity toward both OER and ORR features with low onset overpotentials of 0.21 V and −0.27 V, respectively, with a 0.76 V potential gap between OER potential at 10 mA cm^{-2} and ORR potential at −3 mA cm^{-2}, demonstrating that it is the preeminent bifunctional electrocatalyst reported to date. Compared with pristine NiRu-LDHs, the resulting Ag NP/NiRu-LDHs nanosheets require only an overpotential of 0.31 V to deliver 10 mA cm^{-2} with excellent durability. The superb bifunctional performance of Ag NP/NiRu-LDH is ascribed to the formation of multivacancies, mutual benefits of synergistic effect between metal LDHs and silver nanoparticles, and increased accessible active sites together with site activity are the key to the perceived performance. This work provides a new strategy to decorate LDHs and to engineer multivacancies to enhance site activity and populations simultaneously as ORR/OER bifunctional electrocatalysts.

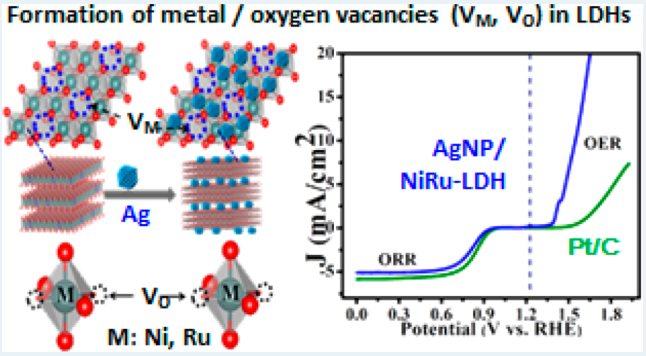

KEYWORDS: *oxygen electrocatalyst, vacancies, site activity, site populations, layered double hydroxides, silver nanoparticles*

Downloaded by ALBRIGHT COLG at 00:13:10:366 on June 18, 2019
from https://pubs.acs.org/doi/10.1021/acscatal.8b03092.

INTRODUCTION

The innovative development of clean and sustainable energy alternatives to fossil fuels has become one of the most pressing issues facing society today. However, large-scale production and storage of clean energy by such alternating sources remains a major challenge.[1,2] Oxygen evolution reaction (OER) and oxygen reduction reaction (ORR) are core reactions in several energy storage and conversion applications and have been considered as the fundamental processes in fuel cells, electrolyzers, and metal−air batteries.[3] Developing effective bifunctional electrocatalysts for ORR/OER is critical in advancing these electrochemical devices toward commercialization because the sluggish kinetics of ORR/OER results in larger overpotential and thus lowers the conversion efficiency.[4−6] Noticeably, the previous research has been performed with Pt, Pd, and Ir-based materials as the ORR catalysts,[7] and IrO_2 and RuO_2 are the most active OER catalysts. Nevertheless, their low earth abundance and high cost prevent these materials from practical applications.

Durable, cost-effective and vastly active bifunctional catalyst for ORR/OER are essential to minimize overpotential and low-quality heat dissipation to increase the energy conversion and utilization efficiency. Especially for the OER, the reaction can be much improved under alkaline conditions, but the

Received: August 3, 2018
Revised: October 18, 2018
Published: November 21, 2018

© 2018 American Chemical Society

DOI: 10.1021/acscatal.8b03092
ACS Catal. 2019, 9, 117−129

durability of electrocatalysts would be greatly declined. In this respect, widespread efforts have been undertaken to search for durable, low-cost, and tremendously active alternatives. Specifically, the catalytic activities of d-block elements for ORR/OER were anticipated to narrate the number of d-electron; where the metal surface exhibited e_g orbitals that can bond with anion adsorbents. Among them, perovskites,[8−10] nickel oxides, or hydroxides[11−13] are the materials that have been often studied. Recently, transition metals, particularly, Ni-based layered double hydroxide (LDHs) have emerged and exhibited promising features.[14−18]

It is already acknowledged that incorporation of other trivalent or tetravalent transition metals such as iron, manganese, chromium, and vanadium into nickel hydroxide ($Ni(OH)_2$) to build LDHs appeared to be crucial for the enhanced activities, although the fundamental role of such metals was unclear in LDHs.[19] Furthermore, there have been no systematic attempts to understand the correlation between the activity of Ni-based LDHs toward the mechanisms, active site of oxygen evolution, and nature of the incorporated metals. Incorporating iron into $Ni(OH)_2$ builds NiFe-LDHs; a promising candidate for OER.[3,20] Besides iron, promising catalytic activities of NiCo-LDHs have also been reported for OER.[21] Nevertheless, the catalytic activity of NiCo-LDHs is reasonably low when compared with NiFe-LDHs under the same conditions.[3,20] The Ni-based layered double hydroxides of transition metals are one of the most OER active and non-noble catalysts in a basic electrolyte.[3,21,22] By contrast, silver nanoparticles are conductive materials and promising candidates for ORR.[23] Instead of designing two separate active sites on the same substrate or exploring proper bifunctional catalytic surface sites, we propose the heterogeneous electrocatalyst of NiRu-LDHs nanosheets decorated with silver nanoparticles to obtain efficient and potential bifunctional catalyst. Even though Ni-based LDHs materials have been extensively conducted as OER electrocatalysts, it is worth mentioning that there has been no reported article for NiRu-LDHs as a catalyst for OER up to now because the sizes of Ru and Ni hydroxides are significantly different. Incorporating Ru into $Ni(OH)_2$ is proposed to produce NiRu-LDHs with multiple vacancies, which is beneficial for catalytic activity.

Herein, we have designed a novel approach to fabricate efficient bifunctional electrocatalyst NiRu-LDHs nanosheets decorated with silver nanoparticles and generated dense and uniform nanosheets of Ag NP/NiRu-LDHs for the first time. In this study, we realized the synthesis of NiRu-LDHs as starting material. It is observed that the NiRu-LDHs nanosheets decorated by silver nanoparticles showed much better bifunctional performance than most catalysts reported in literature. This improvement can be attributed to the mutual benefits of synergistic effects between Ag NPs and LDHs, the formation of multiple vacancies (oxygen vacancy and metal vacancies), the formation of alternative accessible active sites, and conductivity improvement after incorporation of Ag NPs. The fundamental features and practical requirement of Ag NP/NiRu-LDHs toward ORR/OER in alkaline electrolyte were addressed. Even though the Ni-based layered double hydroxides have been made for OER previously,[3,17,18,20] this catalyst was reported for the first time. This work thus aims to provide insight into strategies to design catalysts for their integration in industrially relevant alkaline electrolysis systems and emerging fuel devices. The effect of incorporating ruthenium into $Ni(OH)_2$ on its local structure and catalytic properties were investigated by utilizing advanced spectroscopic techniques and electrochemistry. Interestingly, introducing Ru into $Ni(OH)_2$ provides a novel approach to engineer active site activity and populations via the formation of multiple vacancies. Similarly, the effects of Ag incorporation on NiRu-LDHs structure was simultaneously investigated in both NiRu-LDHs and Ag NP/NiRu-LDHs to fully understand the role of Ag in catalytic activity and stability.

EXPERIMENTAL SECTION

Synthesis of NiRu-LDHs Nanosheets Precursor Phase. In a typical synthesis, NiRu-LDHs were synthesized via hydrothermal methods as previously described for NiFe-LDHs with a simple modification.[3,16,17,20,24] First, $Ni(NO_3)_2 \cdot 6H_2O$ and $Ru(NO)(NO_3)_x \cdot y(OH)$, where $x + y = 3$ with a Ni^{2+}/Ru^{3+} molar ratios equal to 3 are dissolved in a mixed solution of 16 mL of deionized (DI) water and 8 mL of DMF and stirred vigorously for 10 min to form a homogeneous solution. Then urea (16 mmol) was introduced subsequently following addition of 10 mL of 1 M NH_4F under stirring to favor the precipitation and to create alkaline environment. Then the above solution was transferred into Teflon-lined autoclave for hydrothermal treatment and heated at 150 °C in an oven for 12 h. It was then naturally cooled to room temperature, and the resulting product was collected by centrifugation and washed with ethanol and DI water several times, and then finally dried at 80 °C for 6 h.

Synthesis of NiRu-LDHs Nanosheets Decorated with Silver Nanoparticle (Ag NP/NiRu-LDHs). Silver nanoparticles were synthesized using simple procedures previously described in the literature[25−29] with a simple modification. NiRu-LDHs nanosheets decorated with silver nanoparticles were synthesized using previously reported Au NPs deposited on layered double hydroxide as described in the literature[30−32] via hydrothermal methods with a simple modification. Typically, the as-prepared Ag NPs (1.6 mmol) were dispersed into 40 mL of DI water under ultrasonication. Both 2.4 mmol $Ni(NO_3)_2 \cdot 6H_2O$ and 0.8 mmol $Ru(NO)(NO_3)_x \cdot y(OH)$ were dissolved into 40 mL of Ag NPs suspension. Subsequently, 16 mmol of urea was added to the mixture under continuous magnetic stirring, and the homogenized mixture was transferred to the stainless-steel 100 mL Teflon-lined autoclave vessel. The hydrothermal reaction route was performed at 120 for 18 h. After being cooled naturally to room temperature, the composites were separated by centrifugation, cleaned with ethanol and DI water, and then finally dried at 60 °C in a vacuum oven for 12 h. The molar ratio of Ag NPs in Ag NP/NiRu-LDHs was 1:2.

Materials Characterization. Crystal structure of the resulting materials were analyzed using X-ray diffraction (XRD) measurement (XRD-300W with radiation of Cu Kα) under operation conditions of 30 kV and 10 mA. Raman spectra were collected using a confocal Raman microscope integrated by Protrustech Co., Ltd. with a power of 1−3 mW and wavelength of 633 nm. Fourier transform infrared (FT-IR) spectrophotometry (FTS-3500, Bio-Rad, U.S.A.) was taken on by blending the sample into a KBr pellet to provide the functional group information. The diffuse reflectance UV−vis spectra were acquired using JASCO (ISV-469) V 560 UV−vis spectrometer. Morphologies and elemental analysis were investigated by SEM (JSM 6500F, JEOL) integrated with EDX and TEM equipped with EDX on a Titan G2 60−300 transmission electron microscope. XPS (PHI, 1600S) was

DOI: 10.1021/acscatal.8b03092
ACS Catal. 2019, 9, 117−129

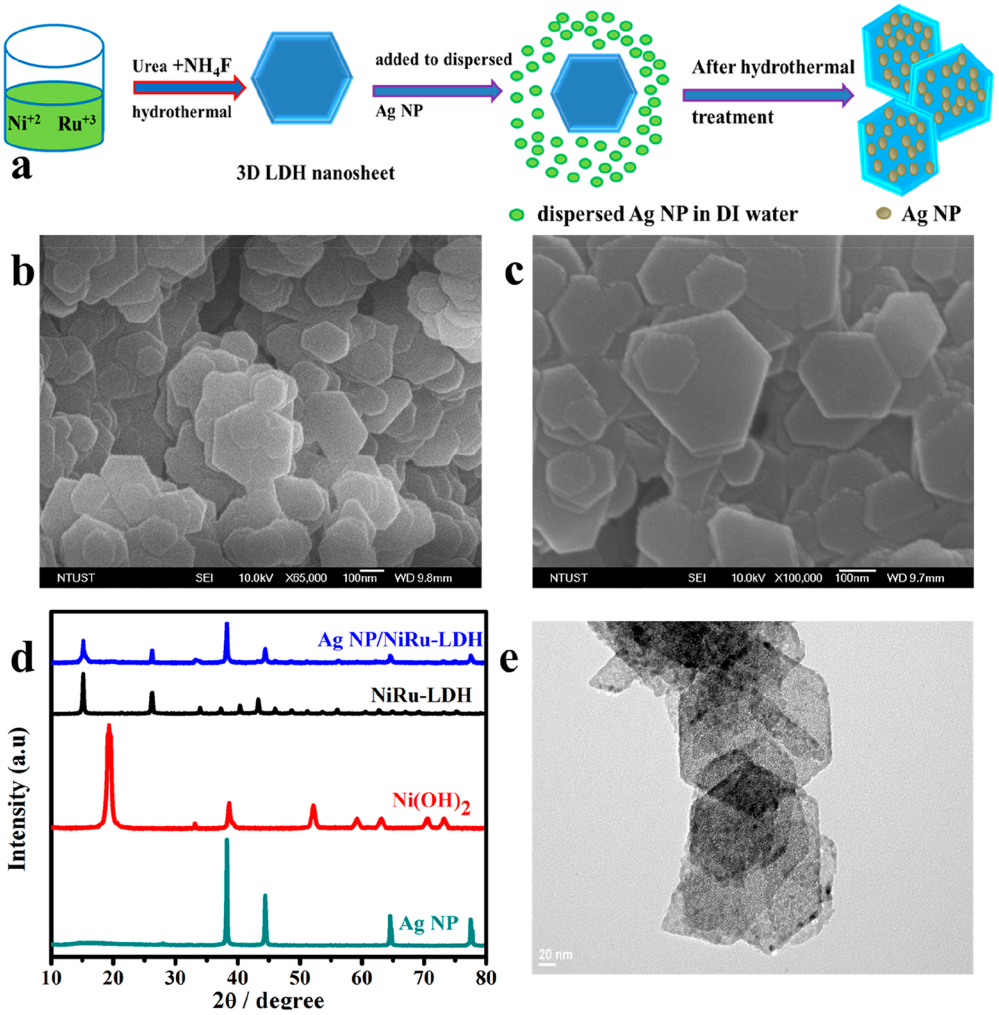

Figure 1. Schematic illustration of NiRu-LDHs nanosheets decorated with conductive Ag NPs fabrication route (a). SEM images of pristine NiRu-LDHs nanosheets (b,c) at lower and higher magnifications, respectively. (d) X-ray diffraction patterns of Ag NPs, β–$Ni(OH)_2$, NiRu-LDHs nanosheets, and Ag NP/NiRu-LDHs for comparison and (e) TEM image of Ag NP/NiRu-LDHs nanosheets.

employed to study the surface composition and recorded at the beamline station of 24A in National Synchrotron Radiation Research Center (NSRRC) in Hsinchu, Taiwan. XAS was conducted at the beamline station BL01C1 in NSRRC Hsinchu, Taiwan. The operation current of the storage ring of the electronic accelerator at 360 mA can supply an electronic energy of 1.5 GeV. The measurements were performed in transmission mode at room temperature, with gas-filled ion chambers being used as X-ray intensity detectors.

Electrochemical Measurements. Electrochemical activity measurements were performed using a computer controlled potentiostat (PGSTAT302N, Metrohm Autolab) assembled with a rotational system (Pine Research Instrumentation, Durham, NC, U.S.A.) with a standard three electrode glass cell (graphite rod as a counter electrode, Ag/AgCl/sat. KCl reference electrode, modified glassy carbon electrode (GCE) with catalysts as the working electrode) in 0.1 M KOH electrolyte at room temperature. The modified GCE was made by casting 14 μL (loading = 70 μg cm^{-2}) of catalyst ink prepared by ultrasonically dispersed 5 mg of catalysts in 1 mL of isopropanol and DI water (3:1) and Nafion solution (70 μL, 0.05 wt % in alcohol) on the surface of pretreated GCE.

RESULTS AND DISCUSSION

Structure and Morphology Characterization. NiRu-LDHs nanosheets and the decoration action was performed by mixing dispersed Ag NPs in DI water and the solution containing metal LDHs via hydrothermal process, as shown in Figure 1a. The hexagonal geometry and interconnected nanosheet-like morphology of NiRu-LDHs was confirmed by scanning electron microscopy (SEM) (Figure 1b,c and Figure S1a–c in Supporting Information (SI)). These nanosheets have a minimum self-aggregation and an open structure which is advantageous for the electrocatalytic reactions.

Figure 1d shows the typical X-ray diffraction patterns (XRD) of Ag NPs, β–$Ni(OH)_2$, NiRu-LDHs, and NiRu-LDHs nanosheets decorated with conductive Ag NPs (Ag NP/NiRu-LDHs). Remarkably, $Ni(OH)_2$ was synthesized without ruthenium precursor using the same synthesis method to further investigate the phase and structural change (Figure 1d, red line). The incorporation of ruthenium into $Ni(OH)_2$ encouraged successful development of LDHs. X-ray diffraction patterns of NiRu-LDHs (Figure 1d) are in good concurrence with Bragg reflections of the known transition metals layered double hydroxide. The diffraction peak of 14.9° (2θ) related to interlayer galleries filled with anions such as OH^-, CO_3^{2-}, NO_3^-, and H_2O molecules to balance the excessive cationic

DOI: 10.1021/acscatal.8b03092
ACS Catal. 2019, 9, 117–129

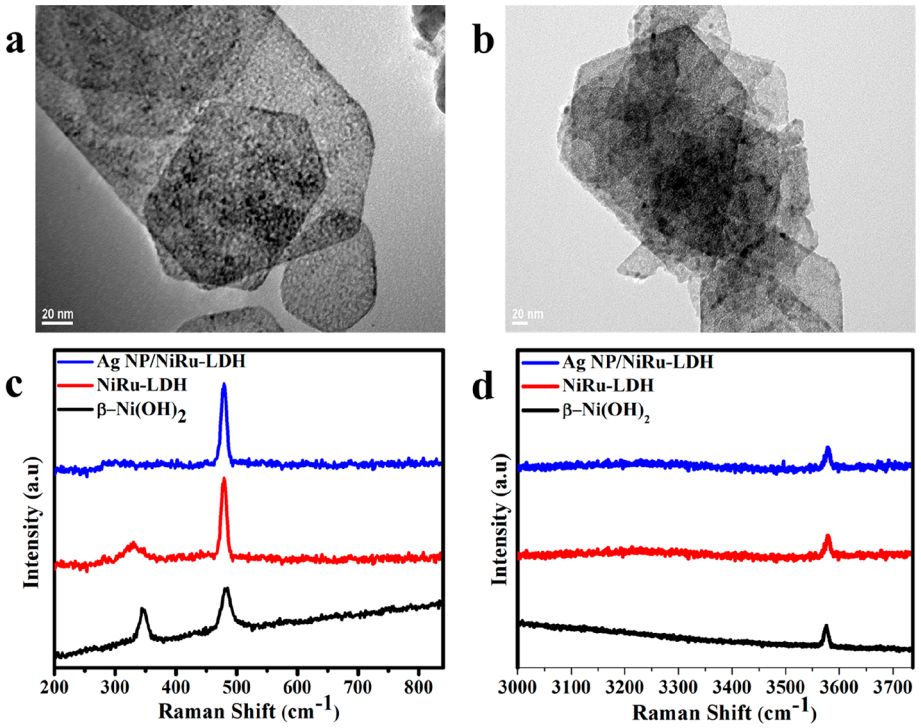

Figure 2. TEM images of the as-prepared Ag NP/NiRu-LDHs nanosheets at different magnifications (a and b). Raman spectra of as-synthesized β–$Ni(OH)_2$, NiRu-LDHs, and Ag NP/NiRu-LDHs (c and d).

charge due to Ru^{3+} between the hydroxide layers. We have also synthesized NiRu(Cl^-)-LDHs and NiRu(NO_3^-)-LDHs (Figure S1d) for comparison to inspect the influence of intercalated anions on crystalline phases of the as-prepared LDHs. The XRD data showed uniform diffraction patterns, which are indicative of ordered crystalline phase. In the X-ray diffraction pattern of NiRu-LDHs decorated with conductive Ag NPs (Figure 1d, blue line), the diffraction peaks of NiRu-LDHs and Ag NPs were superimposed and demonstrate Ag NPs and LDHs compositions were integrated with high crystallinity. The intensity of diffraction patterns of (003) and (006) planes was slightly weakened, but the *d*-spacing did not change obviously, indicating that decoration strategy changes slightly the crystal structure (Table S1). As shown in Figure 1d, the crystal planes of (111), (200), (220), and (311) were indexed in X-ray diffraction pattern of the Ag NPs. Figure S2a indicates SEM image of the well-dispersed silver nanoparticles. The spectroscopic investigation of the as-prepared Ag NPs is displayed in Figure S2b as a function of different time intervals.

The morphology and crystallography of the Ag NP/NiRu-LDHs nanosheets were further obtained from transmission electron microscopy (TEM) images. It reveals that the Ag NP/NiRu-LDHs nanosheets have a sheet-like morphology (Figure 1e and Figure 2a,b), in good agreement with the SEM results. As shown in Figure 1e and Figure 2a,b, the surface of LDHs nanosheets was uniformly decorated with conductive Ag NPs. It seems that many small Ag NPs are intimately decorated on the surface of LDHs nanosheets without obvious aggregation. However, the high-resolution TEM (HRTEM) reveals that the surface of LDHs is not smooth after being decorated, suggesting the presence of distortion or defects. All Ni, Ru, and Ag signals were detected on the surface of LDHs nanosheets decorated with Ag NPs using EDX elemental analysis (Figure S3). This result indicates that the decoration of NiRu-LDHs with conductive Ag NPs was successfully achieved and reliable with the SEM and XRD results, which confirm the crystallography, morphology, and element composition of the obtained Ag NP/NiRu-LDHs nanosheets. Therefore, the as-prepared sample was in fact NiRu-LDHs nanosheets decorated with silver nanoparticles (Ag NP/NiRu-LDHs).

Fourier transform infrared (FT-IR) spectroscopy has been acknowledged to be a useful technique to validate the anions located between the interlayers of the as-prepared Ag NP/NiRu-LDHs (Figure S2c). The strong broad bands at 3669 and 3439 cm^{-1} and a medium band at about 1635 cm^{-1} were recognized as non-hydrogen-bonded OH group stretching vibration, the stretching mode of the OH bonds in the hydroxide layers; OH related to hydrogen bond in H_2O molecules in the interlayer galleries of LDHs; and hydroxyl deformation mode in the interlayer water molecules, respectively.[33,34] The strong band at around 1385 cm^{-1} indicates the asymmetric stretching mode of carbonate anion. The bands between 650−550 cm^{-1} belonged to vibrational stretching of O−M−O, M−O−M, and M−O (M = Ru or Ni). The result obtained from FT-IR spectrum shows the existence of intercalated OH ions, H_2O molecules, and CO_3^{2-}.

Raman spectra of LDHs (Figure 2c) in the region from 250 to 650 cm^{-1}, contained two signals at 330.0 and 479.0 cm^{-1}. The strength of the latter in the spectra suggests a symmetric stretching band. The vibration peaks at 479.0 and 478.7 cm^{-1} are ascribable to the symmetric stretching mode of Ni−O and Ni−OH, demonstrating the typical formation of $Ni(OH)_2$ in both NiRu-LDHs and Ag NP/NiRu-LDHs, respectively.[35] The disordered structure of $Ni(OH)_2$ in NiRu-LDHs featured a weak broad band at ∼330.0 cm^{-1}. This band become broad and very weak after silver nanoparticles decorated on the surface of LDHs nanosheets and this further attributed to disordered structure of Ag NP/NiRu-LDHs. The Raman shifts at 3579.2 and 3578.2 cm^{-1} (Figure 2d) indicates the OH

DOI: 10.1021/acscatal.8b03092
ACS Catal. 2019, 9, 117−129

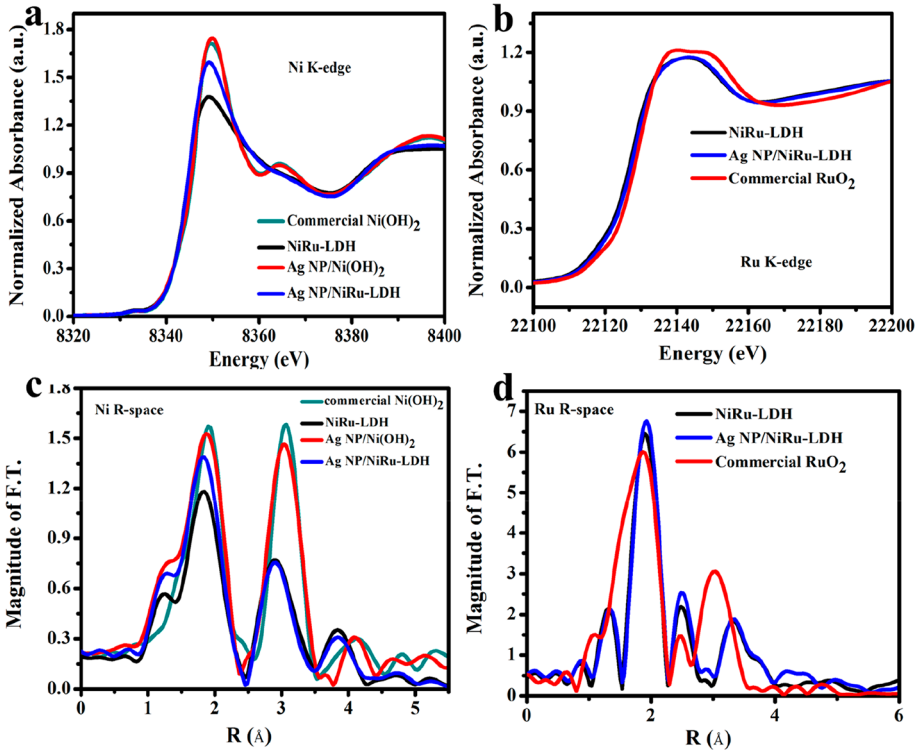

Figure 3. (a) Ni K-edge XANES spectra for NiRu-LDHs, Ag NP/$Ni(OH)_2$, Ag NP/NiRu-LDHs and commercial $Ni(OH)_2$. (b) Ru K-edge XANES spectra of as-prepared NiRu-LDHs, Ag NP/NiRu-LDHs and commercial crystalline RuO_2. (c) Ni K-edge FT-EXAFS spectra of NiRu-LDHs, Ag NP/$Ni(OH)_2$, Ag NP/NiRu-LDHs and commercial $Ni(OH)_2$ samples. (d) Ru K-edge FT-EXAFS spectra of NiRu-LDHs, Ag NP/NiRu-LDHs, and commercial crystalline RuO_2 samples.

stretching of $Ni(OH)_2$ in NiRu-LDHs (Figure 2d, black line) and Ag NP/NiRu-LDHs (Figure 2d, blue line), respectively. Evidently, the vibrational OH stretching of β−$Ni(OH)_2$ was at about ∼3580 cm^{-1}, while α-$Ni(OH)_2$ exhibits a broad band between 3620−3675 cm^{-1}.[19,36] Thus, based on the results obtained from Raman spectra, we deduce that both NiRu-LDHs and Ag NP/NiRu-LDHs nanosheets are composed of β−$Ni(OH)_2$.

The surface chemical states, composition, and valence state elements were assessed using X-ray photoelectron spectroscopy (XPS) before and after decoration was performed (Figure S4 and Table S2). Figure S4 shows XPS spectra of Ni 2p, Ru 3p, and Ag 3d XPS core levels. The Ag 3d spectrum presents two peaks at around 368.5 and 374.4 eV for Ag NPs and Ag NP/NiRu-LDHs (Figure S4a), corresponding to Ag $3d_{5/2}$ and Ag $3d_{3/2}$, respectively, which are characteristics of Ag^0.[37] These finding features show a satisfactory agreement with previous work in which peak broadening of Ag 3d with small shift to a higher and lower binding energy of Ag $3d_{5/2}$ observed when supported on metal oxide due to the charge polarization.[38] The binding energies of Ni 2p for NiRu-LDHs nanosheets were located at 854.3 eV (Ni $2p_{3/2}$) and 872.1 eV (Ni $2p_{1/2}$), while the corresponding peaks of Ni 2p of Ag NP/NiRu-LDHs shift 0.2 eV toward the lower binding energy as shown in Figure S4b accompanied by two shakeup satellites indicate the presence of high-spin Ni^{2+}. The Ru 3p split into Ru $3p_{3/2}$ (461.7 and 461.8 eV) and Ru $3p_{1/2}$ (483.8 and 484.1 eV) in pristine NiRu-LDHs and Ag NP/NiRu-LDHs, respectively, as indicated in Figure S4c, and this signature is characteristic of Ru^{3+}; hence, X-ray photoelectron spectroscopy suggests that Ni and Ru ions are mainly in oxidation states of Ni(II) and Ru(III) in both NiRu-LDHs and Ag NP/NiRu-LDHs, consistent with the values for Ni(II) previously reported in the samples of NiFe-LDHs[39] and Ru(III) in $Ru(acac)_3$.[40] After decorating the surface of LDHs nanosheets with Ag NPs, Ni 2p peaks slightly shifted to lower binding energy. Similarly, the broad peak of Ag 3d with a small shift to a higher and lower binding energy observed after Ag NPs embedded on the surface of LDHs, suggesting the charge polarization due to the charge transfer between Ag and Ni. Thus, the negative shift of Ni binding energy is due to the charge transfer from Ag to Ni sites and confirms the existence of strong electron interactions between Ag and Ni species. The XPS spectra of O 1s peaks (Figure S5) were fitted using Gaussian, and the O 1s spectrum of β-$Ni(OH)_2$ shows three oxygen contributions. The fitted peak at a binding energy of 530.2 eV is a typical metal−oxygen bond. The peak at 531.0 eV is usually associated with oxygen in hydroxide groups. Furthermore, the peak at 531.9 eV can be attributed to the presence of chemisorbed water at or near the surface. However, the curve-fitting of O 1s spectra of both NiRu-LDHs and Ag NP/NiRu-LDHs show four distinct peaks, which can be ascribed to metal−oxygen bonds (lattice oxygen),[41] oxygen in hydroxide groups,[42] oxygen vacancy,[42] and adsorbed water molecules with peaks appearing at binding energies around 529.9, 530.7, 531.4, and 532.2 eV, respectively. These results are similar to the previously reported literatures of XPS O 1s features.[43,44] It has been reported that the O 1s spectra contains two states called oxygen-sufficient states and oxygen-deficient (oxygen vacancy).[45,46] Therefore, the peak at 531.4 eV is associated with the oxygen atoms in the vicinity of oxygen defects and considerably reveals vacant oxygen sites, which come from the structure of LDHs. This result indicates that there are plentiful

DOI: 10.1021/acscatal.8b03092
ACS Catal. 2019, 9, 117−129

Table 1. Local Structure Parameters around Ni Estimated by EXAFS Analysis[a]

samples	shell	N	R (Å)	ΔE_0 (eV)	σ^2 (Å^2)	R-factor ($\times 10^{-3}$)
Ag/Ni(OH)$_2$	Ni−O	6.0 ± 0.405	2.046 ± 0.008	−8.331	0.007	0.4
	Ni−Ni	6.0 ± 0.405	3.123 ± 0.008	−4.927	0.007	
NiRu-LDH	Ni−O	4.338 ± 0.786	2.034 ± 0.018	−6.059	0.007	4.1
	Ni−Ni	2.988 ± 2.520	2.969 ± 0.064	−6.509	0.009	
	Ni−Ru	1.494 ± 1.260	3.168 ± 0.051			
Ag NP/NiRu LDH	Ni−O	5.322 ± 0.624	2.028 ± 0.011	−8.039	0.007	2.1
	Ni−Ni	2.802 ± 2.241	2.960 ± 0.028	−9.900	0.009	
	Ni−Ru	1.401 ± 1.121	3.184 ± 0.035			

[a]N = coordination number; R = distance between absorber and backscatter atoms; σ^2 = Debye−Waller factor; ΔE_0 = energy shift, N of Ni−M (M = Ni, Ru): 4.482 for NiRu-LDH and N_{Ni-O}/N_{Ni-M}: 0.968 whereas, N of Ni−M (M = Ni, Ru): 4.203 for Ag NP/NiRu-LDHs and N_{Ni-O}/N_{Ni-M}: 1.266.

oxygen vacancies in the NiRu-LDHs nanosheets and Ag NP/NiRu-LDH hybrids.

The X-ray absorption spectroscopy (XAS) was employed to deduce coordination number, the local symmetry, and valence state of the surface atoms. As shown in the X-ray absorption near edge structure (XANES) spectra of Ni K-edge for NiRu-LDHs, Ag NP/Ni(OH)$_2$, Ag NP/NiRu-LDHs, and commercial Ni(OH)$_2$ (Figure 3a), obviously all the samples showed a low intensity pre-edge shoulder at around 8333 eV, attributed to electronic transition from 1s to 3d orbital. The strong absorption peak at around 8350 eV for Ni K-edge was due to a dipole transition of 1s orbital to the 4p orbital. Absorption edge positions of Ni-edge of as-prepared NiRu-LDHs, Ag NP/Ni(OH)$_2$ and Ag NP/NiRu-LDHs nanosheets coincide very-well with that of commercial Ni(OH)$_2$, illustrating Ni exists as Ni^{2+} bonded with oxygen in the samples.[47] As shown in Figure 3a, the intensities of Ni K-edge XANES spectra of NiRu-LDHs and Ag NP/NiRu-LDHs decreased relative to the as-prepared Ag NP/Ni(OH)$_2$ and the commercial Ni(OH)$_2$, revealing that the electronic properties around Ni-species were changed. The XANES results provide evidence that there exists Ni^{2+} oxidation state in both NiRu-LDHs and Ag NP/NiRu-LDHs. Figure 3b presents the Ru K-edge XANES spectra of as-prepared NiRu-LDHs, Ag NP/NiRu-LDHs, and commercial RuO_2, and evidently the pre-edge peak is highly sensitive to symmetry and oxidation state and not visible as Ni K-edge. It is worth mentioning that the pre-edge peak of Ru K-edge results from localized (i.e., bound-state) forbidden dipole transitions of 1s → 4d and allowed dipole transitions of 1s → 5p, suggesting that the weak forbidden dipole transition of 1s → 4d peaks overwhelmed by an intense main peak of 1s → 5p. The main edge around 22132 and 22147 eV for Ru k-edge could be attributed to the 1s to 5p and the 1s to 4p transitions, respectively, further illustrating the trivalent oxidation state of Ru in both LDHs and Ag NP/NiRu-LDHs,[48] as evidenced in XPS results and this may attribute to the further orbital hybridization between 3d orbitals of Ni and 2p orbitals of oxygen, which leads to elevating the level of Ru 4d electrons transfer to Ni 3d orbital by Ni−O−Ru, which could stabilize high value Ru ions. In general, octahedral geometry have very low-intensity 1s → nd transition pre-edge features, whereas lower symmetry complexes can have higher-intensity pre-edge features. Therefore, 1s → nd transition pre-edge of both Ni and Ru features good indicators of coordination number and octahedral geometry around the metal center in both NiRu-LDHs and Ag NP/NiRu-LDHs.

The oscillation amplitude of Ni K-edge Re[x(q)] k-space oscillation curves (Figure S6a-c) of the Ag NP/NiRu-LDHs and NiRu-LDHs nanosheets is less than Ni(OH)$_2$. The Fourier transformed (FT) k^3x(k) functions (Figure S6d-f) confirmed and clarified this amplitude reduction. Figure 3c,d show the EXAFS spectra of Ni K-edge and Ru K-edge of both NiRu-LDHs and Ag NP/NiRu-LDHs. The phase-uncorrected EXAFS spectra of Ni K-edge and Ru K-edge display two main peaks: peak I reflecting the presence of M−O (M = Ni or Ru at 1.84 and 1.87 Å, respectively) interactions and peak II manifests M−M (2.90 and 2.30 Å) interactions. The intensity of Ni−O and Ni−M in NiRu-LDHs and Ag NP/NiRu-LDHs decreased significantly compared to the commercial Ni(OH)$_2$ (Figure 3c), suggesting less-ordered structure or smaller nanocrystalline size compared to Ni(OH)$_2$. This result validates the decrease in coordination number (N) around the coordination sphere of Ni−O and Ni−M, indicating that the formation of oxygen vacancies and metal vacancies associated with the size reduction of LDHs by the introduction of Ru.

The structural parameters of the samples can be extracted from the fitting as shown in Table 1 and Figure S6. It demonstrates an octahedral coordination of Ni−O at a distance of 2.028 Å in Ag NP/NiRu-LDHs, which is slightly smaller than the distance of 2.034 and 2.046 Å for pristine NiRu-LDHs and Ag NP/Ni(OH)$_2$, respectively. Meanwhile, the Ni−O coordination number (N) of Ag NP/NiRu-LDHs and NiRu-LDHs is found to be less than Ag NP/Ni(OH)$_2$ (N = 6.00), which is attributed to the existence of oxygen vacancies (V_O). The total coordination numbers of Ni−M was 4.203 in the silver nanoparticles decorated LDHs, lower than the pristine NiRu-LDHs (N = 4.482) and Ag NP/Ni(OH)$_2$ (N = 6.00), revealing the existence of metal vacancies (V_M) in both the pristine NiRu-LDHs and Ag NP/NiRu-LDHs, and the number of metal vacancies in Ag NP/NiRu-LDHs is higher than that in the pristine LDHs. Moreover, the Ag NP/NiRu-LDHs nanosheets exhibited a larger Debye−Waller factor, which also reveals the increased degree of disorder, indicating that the slightly structural distortion occurs around the Ni centers as a result of the oxygen vacancy formation. The Ag NP/NiRu-LDHs nanosheets with the increase of oxygen and metal vacancies, could serve as a catalytically active site and has the contribution to enhance their catalytic performances.[49] Ni(OH)$_2$ is typically used as an efficient OER catalyst. Incorporating Ru into Ni(OH)$_2$ creates multiple vacancies (oxygen vacancies and metal vacancies) associated with the size reduction of LDHs and decorating the surface of LDHs with conductive Ag NPs, further increases the number of accessible active sites. It is believed that Ni is an active site for

DOI: 10.1021/acscatal.8b03092
ACS Catal. 2019, 9, 117−129

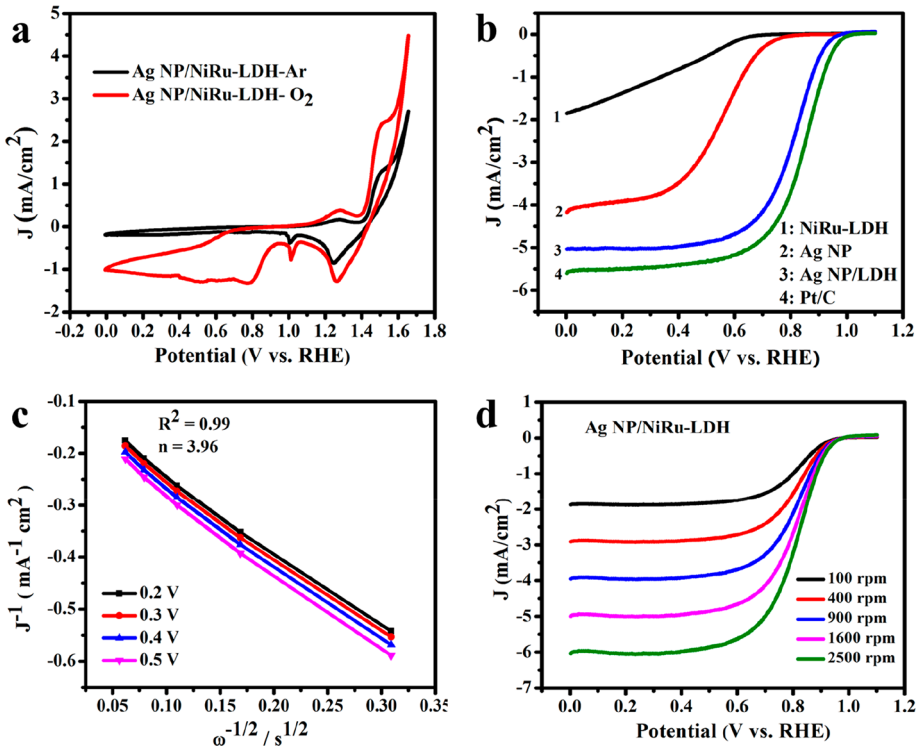

Figure 4. Electrochemical ORR performance of Ag NP/NiRu-LDHs. (a) Cyclic voltammogram plots of Ag NP/NiRu-LDHs nanosheets within ORR and OER potential window in O_2-saturated and Ar-saturated 0.1 M KOH electrolyte. (b) Oxygen reduction LSV curves of Pt/C, Ag NP/NiRu-LDHs, Ag NPs, and NiRu-LDHs at a scan rate of 1 mV s^{-1} and rotating rate of 1600 rpm. (c) Koutecky–Levich plots of Ag NP/NiRu-LDHs derived from LSV curves at different potentials. (d) ORR LSV curves for Ag NP/NiRu-LDHs at various rotating rates.

OER, and Ni with higher oxygen vacancies and metal vacancies could result in higher site activity and site populations.

Bifunctional Performance of the NiRu-LDHs Nanosheets Decorated with Ag NPs. The electrocatalytic activities of as-synthesized materials were investigated using well-prepared rotating disk electrode (RDE). The cyclic voltammogram (CV) of Ag NP/NiRu-LDHs (Figure 4a) shows characterless CV plot in Ar-saturated 0.1 M KOH electrolyte, whereas noticeable cathodic peak perceived at about 0.95 V (vs RHE) in an electrolyte saturated with oxygen, demonstrating that Ag NP/NiRu-LDHs exhibited excellent ORR activity. Both CVs of Ag NP/NiRu-LDHs in O_2-saturated and Ar-saturated electrolytes exhibit three primary characteristics: a redox couple around 1.20, 1.35, and 1.41 V. Nickel-based oxides or hydroxide electrodes feature two well-known characteristic peaks in basic solutions. The anodic peak at lower potentials (~1.35 V) is assigned to the transformation of Ni^{2+}/Ni^{3+}.[3] The Anodic peak found at an overpotential of 1.41 V is attributed to OER, $4OH^- \rightarrow O_2 + 2H_2O + 4e^-$. The anodic wave at about ~1.20 V corresponds to the Ag/Ag^+ redox couple under this condition.[23]

To evaluate ORR activities of Ag NP/NiRu-LDHs, Ag NPs, NiRu-LDHs, and commercial Pt/C, linear sweep voltammetry (LSV) measurements were implemented in O_2-saturated 0.1 M KOH electrolyte with a scan rate of 1 mV/s at 1600 rpm. As shown in Figure 4b, the ORR polarization curves of each catalyst have different limiting currents and onset potentials due to different conductivity and activity, and the onset potential of Ag NP/NiRu-LDHs (~0.96 V) is slightly close to Pt/C (~0.98 V), and is considerably more positive than Ag NPs (~0.81 V) and NiRu-LDHs (~0.70 V). The ORR activity of Ag NP/NiRu-LDHs is significantly better than that for Ag NPs. Although the ORR onset potential of Ag NPs was ~0.81 V, consistent with the previously reported data,[23,50] the onset potential of Ag NP/NiRu-LDHs was about 150 and 260 mV higher than Ag NPs and NiRu-LDHs, respectively, implying excellent ORR activity of Ag NP/NiRu-LDHs. Essentially, limiting current density of Ag NP/NiRu-LDHs (~5.1 mA cm^{-2}) is close to Pt/C, indicating a nearly four-electron transferring pathway.[51] On the contrary, the limiting current density of Ag NPs is far less than 5 mA cm^{-2}, demonstrating that Ag NPs might proceed the ORR via two-electron transferring pathway with the formation of peroxide intermediate.

To further understand the mechanism and nature of the intermediate products via the careful calculation of transferred electrons (n) during ORR test, the limiting current densities at various rotation speeds are used to construct the Levich plots using Koutecky–Levich equation,[51] presented in Figure 4c for Ag NP/NiRu-LDHs. Depending on the slopes of the Levich plots, n was calculated as ~3.96 at 0.2–0.5 V, indicating excellent ORR catalytic activity of Ag NP/NiRu-LDHs via a nearly four-electron pathway. As shown in Figure 4d, LSV measurements were performed at various rotating speeds in the range of 100–2500 rpm to gain further comprehension into ORR mechanisms and kinetics, and it can be realized that as the rotation speeds increased, the diffusion limiting current densities were significantly increased because of shortened diffusion distance of O_2-saturated electrolyte at high speeds. Accordingly, Ag NP/NiRu-LDHs exhibited a smaller ORR Tafel slope than Ag NPs (Figure S7), and this could be due to the best reaction kinetics of these nanosheets and smaller diameter of the semicircle of Nyquist plots for Ag NP/NiRu-LDHs (Figure S8) describes smaller charge transferring

DOI: 10.1021/acscatal.8b03092
ACS Catal. 2019, 9, 117–129

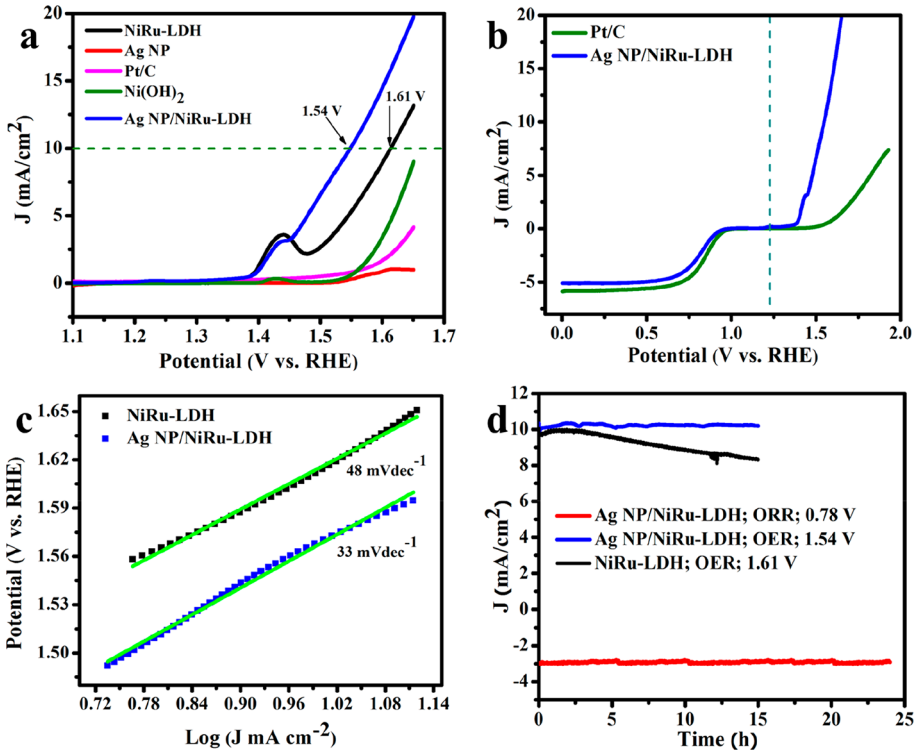

Figure 5. (a) LSV curves of OER activity for different catalysts evaluated in 0.1 M KOH at rotating speed of 1600 rpm. (b) Bifunctional catalytic activity of Ag NP/NiRu-LDHs and commercial Pt/C catalysts toward ORR/OER activities. (c) OER Tafel plots. (d) Chronoamperometric curves of pristine NiRu-LDHs and Ag NP/NiRu-LDHs electrodes carried out under constant potentials of corresponding to −3 mA cm^{-2} and 10 mA cm^{-2}.

resistance. This information suggests that the kinetics and charge transfer for ORR is much better in Ag NP/NiRu-LDHs than Ag or NiRu-LDHs individually. This indicates the advantages of enhanced site activity and accessible site populations considerably improve the ORR activity as discussed in the previous sections. The ORR site activity and populations are mainly contributed from the synergetic effects including; charge polarization occurred on the Ag sites and the presence of LDHs to weaken the adsorption of OH and remove the adsorbed OH from the Ag sites, and the dispersion of Ag to increase the accessible site populations. Moreover, the OH preferably migrated to vacant metal sites of LDHs, which possibly enhances the Ag site activity. Additionally, the presence of multiple vacancies (oxygen and metal) can decrease the adsorption energy of OH*, OOH*, and O* intermediates at the Ag sites and facilitate adsorption of these intermediates.[52,53] Likewise, there are reported literature about transition metal hydr(oxy)oxide cocatalysts with novel catalyst to further improve the ORR catalytic activity. For example, a recent report by Subbaraman et al. established that the combination of precious metal catalysts and oxophilic transition metal hydr(oxy)oxide cocatalysts led to a significantly improved catalytic activity due to OH adsorb preferentially on transition metal (3d−M) hydr(oxy)oxide.[54] It is also well-known that transition metal (3d) hydr(oxy)oxide typically has high ability of water activation to supply proton ($M + xH_2O \rightarrow M\text{-}[OH]_x + xH^+ + xe^-$), which is essential for oxygen reduction to OH^- in alkaline electrolyte.[55] Thus, we also anticipated that the presence of layered double hydroxide in Ag NP/NiRu-LDHs hybrid possibly enhances the water activation ability of the catalyst, which in turn plays a key role in determining the ORR kinetics and improving ORR activity in alkaline condition. Therefore, NiRu-LDHs with multiple vacancies affect both water activation and OH adsorption, which enhances the intrinsic activity. These strong synergetic effects between Ag and LDHs significantly enhanced overall ORR catalytic activity.

The OER performances of Ag NP/NiRu-LDHs, NiRu-LDHs, $Ni(OH)_2$, commercial Pt/C, and Ag NPs were assessed by LSV measurements under the same condition within a potential window of 1.1 to 1.7 V in 0.1 M KOH. The OER polarization curves (Figure 5a) show that the onset potentials were 1.44, 1.48, 1.52, and 1.50 V for Ag NP/NiRu-LDHs, NiRu-LDHs, $Ni(OH)_2$, and Pt/C, respectively. Ag NP/NiRu-LDHs electrode exhibits the earliest onset potential and highest OER activity. Though Dai et al. groups synthesized NiFe-LDH/CNT in 2013 and the material exhibits a lower onset potential of 1.45 V, the concentration of the KOH electrolyte was 1 M, different from 0.1 M used in the current work.[3] Ag NP/NiRu-LDHs exhibits considerably higher OER performance, and the enhanced activity is originated from the improvement of its site activity and populations as a result of the formation of multiple vacancies, the enhancement of conductivity, and the charge transferring effect in the composites.[56] The small oxidation process noticed at around ∼1.39 V (vs RHE) before the OER onset potential is corresponding to the oxidative conversion of $Ni(OH)_2$ to NiOOH species, which are believed to be the active sites that catalyze OER, commonly found in Ni-based OER catalysts.[3] Furthermore, the redox peak potential of Ni^{2+}/Ni^{3+} of NiRu-LDHs exhibited slightly a negative shift compared to bare $Ni(OH)_2$ (Figure 5a), implying the enhanced oxidation of Ni in the NiRu-LDHs. It has been well acknowledged that the less suppressed oxidative potential of Ni^{2+}/Ni^{3+}, or the enlarge-

DOI: 10.1021/acscatal.8b03092
ACS Catal. 2019, 9, 117−129

ment of the average oxidation state of Ni, results in better OER activity. The negatively shifted Ni^{2+}/Ni^{3+} peak potential of NiRu-LDHs could be caused by the formation of oxygen vacancies on Ni sites associated with the changes in its local structure and electronic structure by the introduction of Ru.

As Ag NPs are incorporated into the NiRu-LDHs nanosheets, the redox peak of Ni^{2+}/Ni^{3+} is slightly suppressed to larger potential and rapid rise in the region of OER potential. The commercial Pt/C afforded an onset potential comparable with $Ni(OH)_2$; however, its current density is inferior to our NiRu-LDHs and Ag NP/NiRu-LDHs. Analogous to ORR, the OER catalytic activity also is affected by incorporated Ag NPs as the Ag NP/NiRu-LDHs catalyst shows a smaller Tafel slope and a decreased overpotential. Furthermore, the catalytic activity of NiRu-LDHs nanostructures can be significantly enhanced after silver nanoparticles are decorated on the surface of LDHs nanosheets, as shown by an even higher current density and lowest onset overpotential for both OER and ORR. Specifically, Ag NP/NiRu-LDHs require only 0.31 V overpotential to deliver 10 mA cm^{-2} current density, whereas NiRu-LDHs require 0.38 V. This activity improvement suggests the reaction kinetics for Ag NP/NiRu-LDHs nanosheets is more favorable than the NiRu-LDHs nanosheets. The synergetic effects between metals of layered double hydroxide catalysts underlying Ag NPs, including the generation of oxygen and metal vacancies on Ni sites and the size reduction of LDHs contribute to the enhanced Ni site activity together with site populations and the overall OER catalytic performance. These results are considerably better than earth-abundant metal-based catalysts reported to date[3,21,57] and comparable to that of IrO_2.[58]

The bifunctional catalytic capability of both Ag NP/NiRu-LDHs and Pt/C catalysts toward OER/ORR in alkaline conditions are juxtaposed and compared within identical potential window (Figure 5b). Evidently, Ag NP/NiRu-LDHs exhibited outstanding OER activity and lowest overpotential among these catalysts. The bifunctional performance of Ag NP/NiRu-LDHs is usually assessed by the potential difference (ΔE) between OER overpotential at the current density of 10 mA cm^{-2} and ORR overpotential corresponding to the current density of −3 mA cm^{-2}. Accordingly, Ag NP/NiRu-LDHs exhibited a ΔE value of 0.76 V (vs RHE), further revealing the outstanding bifunctional activity. The key parameters for reported metal-based bifunctional catalysts are listed in Table S3 for comparison.[59] Clearly, Ag NP/NiRu-LDHs demonstrates itself as a promising oxygen electrocatalyst, showing great potential to be applied in rechargeable metal-based air batteries.

To further comprehend the reason behind the superb bifunctional activities of Ag NP/NiRu-LDHs, the electrochemical active surface area (ECSA) of Ag NP/NiRu-LDHs, NiRu-LDHs, and $Ni(OH)_2$ was acquired in nonfaradic region of CV curves at different scanning rates in 0.1 M KOH (Figure S9a-c). The differences in current densities (ΔJ) against scan rates at 0.71 V were plotted (Figure S9d). The double layer capacitance (C_{dl}) of the material can be derived from the half value of the linear slope, which typically indicates the corresponding ECSA.[22,49,60] The slope of Ag NP/NiRu-LDHs (0.562) is much higher than the NiRu-LDHs (about 0.251), indicating that the Ag NP/NiRu-LDHs nanosheets have larger active surface areas than the pristine NiRu-LDHs. The increased ECSA in Ag NP/NiRu-LDHs was attributed to the increased accessible site populations after the introduction of Ru and Ag NPs as result of the improvement of conductivity and the formation of metal vacancies along with the size reduction of LDHs. The correlation of ECSA with the current density of Ag NP/NiRu-LDHs, NiRu-LDHs, and $Ni(OH)_2$ is presented in Figure S9e. The current density increases simultaneously with the increase of the double layer capacitance, further confirming that the ECSA representing active site population is also one of the main factors for catalytic activities. Thus, incorporating a transition metal such as Ru into $Ni(OH)_2$ and the decoration strategy of NiRu-LDHs with Ag NPs effectively increase the site activity and populations and then naturally enhance catalytic activity. Furthermore, the OER polarization curves of each catalyst were normalized for ECSA to evaluate the intrinsic activity improvement of Ni sites. As shown in Figure S9f, after the ECSA has been corrected for the OER polarization curves, still the OER activity of NiRu-LDHs decorated with the silver nanoparticle is much better than the pristine NiRu-LDHs and $Ni(OH)_2$, suggesting the improved site activity of the Ni sites. Thus, we find that the introduction of Ru into $Ni(OH)_2$ enhances the site activity of Ni sites, and the decoration strategy further improves the intrinsic activity of the Ni sites in addition to the increase of site populations.

Tafel slope was used to assess the kinetics of the OER. It is evident to note that a NiRu-LDHs nanosheets decorated with Ag NPs exhibited Tafel slope of 33 mV dec^{-1}, much lower than the NiRu-LDHs nanosheets (48 mV dec^{-1}) (Figure 5c). Hence, the lowest Tafel slope suggested the best reaction kinetics for oxygen evolution and rapid electron transference among all the active materials of interest. The significant difference in intrinsic reaction kinetics between Ag NP/NiRu-LDHs nanosheets and pristine NiRu-LDHs samples also contributes to the different catalytic performance. Increasing active site activity and populations resulting from the formation of multiple vacancies and conductivity enhance the superior reaction kinetics.

Besides the high ORR/OER activities, Ag NP/NiRu-LDHs displayed prominent stability in 0.1 M KOH solution as shown in Figure 5d. It was observed that Ag NP/NiRu-LDHs was capable of maintaining a current density of about 10 mA cm^{-2} at a constant applied potential of 1.54 V with insignificant change for over 15 h under OER condition. Similarly, negligible degradation of the current density corresponding to ORR half-wave potential was achieved for 24 h, demonstrating excellent durability of Ag NP/NiRu-LDHs nanosheets toward ORR/OER activity. The stability test of pristine NiRu-LDHs was also performed under the same condition using chronoamperometric measurements. In Figure 5d, NiRu-LDHs catalyst was unable to maintain the current density of about 10 mA cm^{-2} at a constant potential of 1.61 V, indicating decreased activity during OER. However, the stability of NiRu-LDHs nanosheets has been significantly improved after the decoration of Ag NPs. We believe that the decorated Ag NPs help to reduce the overpotential and then prevent catalytically active sites from degradation.

Discussion of the Enhanced Bifunctional Performance of Ag NP/NiRu-LDHs. Although the correlation between OER activity and metal/oxygen vacancies have been recently reported,[49,60] the relationship between V_O and onset overpotential of the site activity is still lacking. The estimation was based on aforementioned experiments, and the measured values are summarized in Table S4. Details about the calculation and obtained values can be found in Table S5.

DOI: 10.1021/acscatal.8b03092
ACS Catal. 2019, 9, 117−129

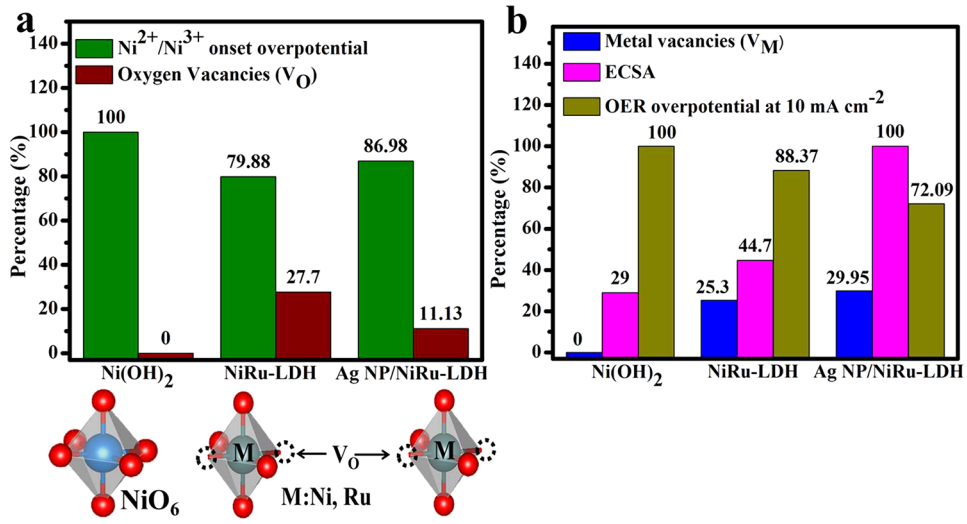

Figure 6. (a) Percentage of oxygen vacancies and Ni site activities. (b) Metal vacancies, ECSA, and OER site activity and site number at the current density of 10 mA cm^{-2} for $Ni(OH)_2$, NiRu-LDHs, and Ag NP/NiRu-LDHs for comparison. The V_O and V_M were estimated from the coordination number (N) of NiRu-LDHs and Ag NP/NiRu-LDHs relative to the N of $Ni(OH)_2$ (= 6) almost equal to the theoretical value.

Figure 6 presents incorporation of Ru into $Ni(OH)_2$ generates NiRu-LDHs with multiple vacancies, accessible electrochemically active surface area, and higher site activity.

Furthermore, Figure 6a shows the percentage of onset overpotential of Ni^{2+}/Ni^{3+} and V_O for $Ni(OH)_2$, NiRu-LDHs, and Ag NP/NiRu-LDHs, indicating that NiRu-LDHs with more V_O possesses lower percentage of onset overpotential of Ni^{2+}/Ni^{3+} than the counterparts, suggesting the higher site activity of NiRu-LDHs. The induced V_O can decline the interference of H_2O adsorption on the surface of the catalyst, leading to increase the activity of site activity and improve OER activity of NiRu-LDHs. Although the Ag decoration strategy slightly decreases V_O, the formation of more metal vacancies associated with the size reduction of LDHs increase the accessible active sites (Figure 6b). Thus, the ECSA was appreciably enhanced after the introduction of Ru and Ag NPs. Furthermore, Ni sites with metal vacancies together with oxygen vacancies act as the centers of water activation, favoring dissociation of H_2O molecules by increasing active site activity and populations. As a result, Ag NP/NiRu-LDHs exhibited lower OER onset potential and lower overpotential at the current density of 10 mA cm^{-2}.

The catalytic activity of $Ni(OH)_2$ can be significantly enhanced after the introduction of Ru as NiRu-LDHs, and the bifunctional activity of this material is further enhanced after silver nanoparticles are decorated on the surface of LDHs nanosheets, as shown by higher current densities and an even lower onset overpotential of ORR/OER. The higher ORR activity of Ag NP/NiRu-LDH was mainly attributed to the increased Ag site activity and accessible Ag site populations. The increased Ag site activity is extensively contributed from the charge polarization occurring on the Ag sites responsible for weakening the adsorption of OH on the Ag sites, and the presence of LDHs helps to remove the adsorbed OH from the surface of Ag. Furthermore, the decoration strategy enhances the dispersion of Ag and considerably increased the accessible site populations. These strong synergetic effects between Ag and LDHs significantly enhanced the catalytic activity of ORR. The increased in OER activity of Ag NP/NiRu-LDHs is attributed to intrinsically active Ni sites with multiple vacancies responsible for the enhanced Ni site activity and accessible Ni site populations particularly after decoration strategy. The strong synergetic effects of silver nanoparticles and metal LDHs engineer the active site activity and populations on both Ag and Ni in the bifuctional electrocatalysts for ORR and OER, respectively. The extraordinary low overpotential for ORR/OER is ascribed to the synergetic effects between Ag NPs and NiRu-LDHs. With low overpotential, low charge-transfer resistance, small Tafel slope and superior durability, the silver nanoparticles decorated on the surface of NiRu-LDHs nanosheets can be an ideal electrocatalyst for ORR/OER.

CONCLUSIONS

Decorating Ag NPs on the surface of NiRu-LDHs nanosheets has been demonstrated as an efficient bifunctional ORR/OER electrocatalyst for the first time. It is interesting to note that the incorporation of Ru into $Ni(OH)_2$ and decoration was accompanied by generating multiple vacancies via a hydrothermal route. These multiple vacancies can effectively increase the site activity and populations of both NiRu-LDHs and Ag NP/NiRu-LDHs nanosheets. The high intrinsic bifunctional catalytic activity of NiRu-LDHs nanosheets decorated with Ag NPs is mainly due to the presence of multiple vacancies and the mutual benefits of strong synergetic effect between LDHs and Ag NPs, which effectively tune the site activity and populations of NiRu-LDHs catalysts. The formation of high intrinsic site activity and accessible site populations on the surface of Ag NP/NiRu-LDHs significantly enhances the reaction kinetics. In addition, Ag NP/NiRu-LDHs also has superior stability due to the incorporation of conductive Ag NPs and resultant synergies. The bifunctional activity of Ag NP/NiRu-LDHs in basic solution outperformed the precious metals that were not able to achieve with low overpotential before. This cheaper and active ORR/OER catalyst offers an advanced solution for energy applications such as metal-air batteries. On the basis of these results, the strategy we developed here also provides a new way to engineer the vacancies of Ni-based materials. Therefore, the strategy might produce non-noble, durable, and highly competitive bifunctional electrocatalysts for ORR and OER.

DOI: 10.1021/acscatal.8b03092
ACS Catal. 2019, 9, 117−129

■ ASSOCIATED CONTENT

Supporting Information

The Supporting Information is available free of charge on the ACS Publications website at DOI: 10.1021/acscatal.8b03092.

SEM images of NiRu-LDHs at different magnification, XRD patterns of NiRu-LDHs, the table containing estimated fwhm and *d*-spacing of NiRu-LDHs and Ag NP/NiRu-LDHs, SEM image of Ag NPs and the corresponding UV−visible spectra, FT-IR spectra of Ag NP/NiRu-LDHs, TEM images and EDX elemental analysis of Ag NP/NiRu-LDHs, XPS spectra and the corresponding elemental compositions, fitting results of the extended XANES and FT-EXAFS of Ni K-edge for Ag NP/$Ni(OH)_2$, NiRu-LDHs and Ag NP/NiRu-LDHs samples, Tafel plots, Nyquist plots, cyclic voltammetry curves obtained in non-Faradaic region and the derived ECSA, the table containing reported literatures and our materials for comparison, the table containing the estimated site activity and site populations (PDF)

■ AUTHOR INFORMATION

Corresponding Authors

*E-mail: bjh@mail.ntust.edu.tw.
*E-mail: wsu@mail.ntust.edu.tw.
*E-mail: hdail@stanford.edu.

ORCID

Wei-Nien Su: 0000-0003-1494-2675
Min-Hsin Yeh: 0000-0002-6150-4750
Cheng-Yen Wen: 0000-0002-9788-4329
Hongjie Dai: 0000-0002-4906-4502
Bing-Joe Hwang: 0000-0002-3873-2149

Notes

The authors declare no competing financial interest.

■ ACKNOWLEDGMENTS

This work was financially supported by the Ministry of Science and Technology (MoST) (106-2923-E 011-005, 105-3113-E-011-001, 105-ET-E-011-004-ET, 104-2923-M-011-002-MY3, 104-2911-1-011-505-MY2, 103-2221-E-011-156-MY3), the Top University Projects (100H45140), the Global Networking Talent 3.0 Plan (NTUST 104DI005) from the Ministry of Education of Taiwan, Taiwan's Deep Decarbonization Pathways toward a Sustainable Society Project (AS-KPQ-106-DDPP) from Academia Sinica as well as the facilities of support from National Taiwan University of Science and Technology (NTUST) and National Synchrotron Radiation Research Centre (NSRRC) are also acknowledged.

■ REFERENCES

(1) Trześniewski, B. J.; Diaz-Morales, O.; Vermaas, D. A.; Longo, A.; Bras, W.; Koper, M. T. M.; Smith, W. A. In Situ Observation of Active Oxygen Species in Fe-Containing Ni-Based Oxygen Evolution Catalysts: The Effect of pH on Electrochemical Activity. *J. Am. Chem. Soc.* **2015**, *137* (48), 15112−15121.

(2) Klaus, S.; Cai, Y.; Louie, M. W.; Trotochaud, L.; Bell, A. T. Effects of Fe Electrolyte Impurities on Ni(OH)2/NiOOH Structure and Oxygen Evolution Activity. *J. Phys. Chem. C* **2015**, *119* (13), 7243−7254.

(3) Gong, M.; Li, Y.; Wang, H.; Liang, Y.; Wu, J. Z.; Zhou, J.; Wang, J.; Regier, T.; Wei, F.; Dai, H. An Advanced Ni−Fe Layered Double Hydroxide Electrocatalyst for Water Oxidation. *J. Am. Chem. Soc.* **2013**, *135* (23), 8452−8455.

(4) Lee, J. S.; Tai Kim, S.; Cao, R.; Choi, N. S.; Liu, M.; Lee, K. T.; Cho, J. Metal−air batteries with high energy density: Li−air versus Zn−air. *Adv. Energy Mater.* **2011**, *1* (1), 34−50.

(5) Ge, X.; Sumboja, A.; Wuu, D.; An, T.; Li, B.; Goh, F. W. T.; Hor, T. S. A.; Zong, Y.; Liu, Z. Oxygen Reduction in Alkaline Media: From Mechanisms to Recent Advances of Catalysts. *ACS Catal.* **2015**, *5* (8), 4643−4667.

(6) Enman, L. J.; Burke, M. S.; Batchellor, A. S.; Boettcher, S. W. Effects of Intentionally Incorporated Metal Cations on the Oxygen Evolution Electrocatalytic Activity of Nickel (Oxy)hydroxide in Alkaline Media. *ACS Catal.* **2016**, *6* (4), 2416−2423.

(7) Gewirth, A. A.; Thorum, M. S. Electroreduction of dioxygen for fuel-cell applications: materials and challenges. *Inorg. Chem.* **2010**, *49* (8), 3557−3566.

(8) Wang, B. Recent development of non-platinum catalysts for oxygen reduction reaction. *J. Power Sources* **2005**, *152*, 1−15.

(9) Takeguchi, T.; Yamanaka, T.; Takahashi, H.; Watanabe, H.; Kuroki, T.; Nakanishi, H.; Orikasa, Y.; Uchimoto, Y.; Takano, H.; Ohguri, N.; Matsuda, M.; Murota, T.; Uosaki, K.; Ueda, W. Layered Perovskite Oxide: A Reversible Air Electrode for Oxygen Evolution/Reduction in Rechargeable Metal-Air Batteries. *J. Am. Chem. Soc.* **2013**, *135* (30), 11125−11130.

(10) Hardin, W. G.; Slanac, D. A.; Wang, X.; Dai, S.; Johnston, K. P.; Stevenson, K. J. Highly active, nonprecious metal perovskite electrocatalysts for bifunctional metal−air battery electrodes. *J. Phys. Chem. Lett.* **2013**, *4* (8), 1254−1259.

(11) Burke, M. S.; Enman, L. J.; Batchellor, A. S.; Zou, S.; Boettcher, S. W. Oxygen evolution reaction electrocatalysis on transition metal oxides and (oxy) hydroxides: Activity trends and design principles. *Chem. Mater.* **2015**, *27* (22), 7549−7558.

(12) Batchellor, A. S.; Boettcher, S. W. Pulse-electrodeposited Ni−Fe (oxy) hydroxide oxygen evolution electrocatalysts with high geometric and intrinsic activities at large mass loadings. *ACS Catal.* **2015**, *5* (11), 6680−6689.

(13) Gong, M.; Dai, H. A mini review of NiFe-based materials as highly active oxygen evolution reaction electrocatalysts. *Nano Res.* **2015**, *8* (1), 23−39.

(14) Oliver-Tolentino, M. A.; Vázquez-Samperio, J.; Manzo-Robledo, A.; González-Huerta, R. d. G.; Flores-Moreno, J. L.; Ramírez-Rosales, D.; Guzmán-Vargas, A. An Approach to Understanding the Electrocatalytic Activity Enhancement by Superexchange Interaction toward OER in Alkaline Media of Ni−Fe LDH. *J. Phys. Chem. C* **2014**, *118* (39), 22432−22438.

(15) Yu, X.; Zhang, M.; Yuan, W.; Shi, G. A high-performance three-dimensional Ni−Fe layered double hydroxide/graphene electrode for water oxidation. *J. Mater. Chem. A* **2015**, *3* (13), 6921−6928.

(16) Long, X.; Li, J.; Xiao, S.; Yan, K.; Wang, Z.; Chen, H.; Yang, S. A strongly coupled graphene and FeNi double hydroxide hybrid as an excellent electrocatalyst for the oxygen evolution reaction. *Angew. Chem.* **2014**, *126* (29), 7714−7718.

(17) Song, F.; Hu, X. Exfoliation of layered double hydroxides for enhanced oxygen evolution catalysis. *Nat. Commun.* **2014**, *5*, 4477.

(18) Trotochaud, L.; Young, S. L.; Ranney, J. K.; Boettcher, S. W. Nickel−iron oxyhydroxide oxygen-evolution electrocatalysts: The role of intentional and incidental iron incorporation. *J. Am. Chem. Soc.* **2014**, *136* (18), 6744−6753.

(19) Louie, M. W.; Bell, A. T. An Investigation of Thin-Film Ni−Fe Oxide Catalysts for the Electrochemical Evolution of Oxygen. *J. Am. Chem. Soc.* **2013**, *135* (33), 12329−12337.

(20) Lu, Z.; Xu, W.; Zhu, W.; Yang, Q.; Lei, X.; Liu, J.; Li, Y.; Sun, X.; Duan, X. Three-dimensional NiFe layered double hydroxide film for high-efficiency oxygen evolution reaction. *Chem. Commun.* **2014**, *50* (49), 6479−6482.

(21) Liang, H.; Meng, F.; Cabán-Acevedo, M.; Li, L.; Forticaux, A.; Xiu, L.; Wang, Z.; Jin, S. Hydrothermal continuous flow synthesis and exfoliation of NiCo layered double hydroxide nanosheets for enhanced oxygen evolution catalysis. *Nano Lett.* **2015**, *15* (2), 1421−1427.

DOI: 10.1021/acscatal.8b03092
ACS Catal. 2019, 9, 117−129

(22) Fan, K.; Chen, H.; Ji, Y.; Huang, H.; Claesson, P. M.; Daniel, Q.; Philippe, B.; Rensmo, H.; Li, F.; Luo, Y.; Sun, L. Nickel−vanadium monolayer double hydroxide for efficient electrochemical water oxidation. *Nat. Commun.* **2016**, *7*, 11981.
(23) Singh, P.; Buttry, D. A. Comparison of Oxygen Reduction Reaction at Silver Nanoparticles and Polycrystalline Silver Electrodes in Alkaline Solution. *J. Phys. Chem. C* **2012**, *116* (19), 10656−10663.
(24) Gao, M.; Sheng, W.; Zhuang, Z.; Fang, Q.; Gu, S.; Jiang, J.; Yan, Y. Efficient Water Oxidation Using Nanostructured α-Nickel-Hydroxide as an Electrocatalyst. *J. Am. Chem. Soc.* **2014**, *136* (19), 7077−7084.
(25) Iravani, S.; Korbekandi, H.; Mirmohammadi, S.; Zolfaghari, B. Synthesis of silver nanoparticles: chemical, physical and biological methods. *Research in pharmaceutical sciences* **2014**, *9* (6), 385.
(26) Li, J.; Kuang, D.; Feng, Y.; Zhang, F.; Xu, Z.; Liu, M.; Wang, D. Green synthesis of silver nanoparticles−graphene oxide nanocomposite and its application in electrochemical sensing oftryptophan. *Biosens. Bioelectron.* **2013**, *42*, 198−206.
(27) El-Nour, K. M. A.; Eftaiha, A. a.; Al-Warthan, A.; Ammar, R. A. Synthesis and applications of silver nanoparticles. *Arabian J. Chem.* **2010**, *3* (3), 135−140.
(28) Abbasi, E.; Milani, M.; Fekri Aval, S.; Kouhi, M.; Akbarzadeh, A.; Tayefi Nasrabadi, H.; Nikasa, P.; Joo, S. W.; Hanifehpour, Y.; Nejati-Koshki, K.; Samiei, M. Silver nanoparticles: synthesis methods, bio-applications and properties. *Crit. Rev. Microbiol.* **2016**, *42* (2), 173−180.
(29) Khan, Z.; Al-Thabaiti, S. A.; Obaid, A. Y.; Al-Youbi, A. Preparation and characterization of silver nanoparticles by chemical reduction method. *Colloids Surf., B* **2011**, *82* (2), 513−517.
(30) Ballarin, B.; Mignani, A.; Scavetta, E.; Giorgetti, M.; Tonelli, D.; Boanini, E.; Mousty, C.; Prevot, V. Synthesis route to supported gold nanoparticle layered double hydroxides as efficient catalysts in the electrooxidation of methanol. *Langmuir* **2012**, *28* (42), 15065−15074.
(31) Mignani, A.; Ballarin, B.; Giorgetti, M.; Scavetta, E.; Tonelli, D.; Boanini, E.; Prevot, V.; Mousty, C.; Iadecola, A. Heterostructure of Au Nanoparticles NiAl Layered Double Hydroxide: Electrosynthesis, Characterization, and Electrocatalytic Properties. *J. Phys. Chem. C* **2013**, *117* (31), 16221−16230.
(32) Varade, D.; Haraguchi, K. Efficient approach for preparing gold nanoparticles in layered double hydroxide: synthesis, structure, and properties. *J. Mater. Chem.* **2012**, *22* (34), 17649−17655.
(33) Ruano-Casero, R.; Pérez-Bernal, M.; Rives, V. Preparation and properties of nickel and iron oxides obtained by calcination of layered double hydroxides. *Z. Anorg. Allg. Chem.* **2005**, *631* (11), 2142−2150.
(34) Zhou, L.-J.; Huang, X.; Chen, H.; Jin, P.; Li, G.-D.; Zou, X. A high surface area flower-like Ni−Fe layered double hydroxide for electrocatalytic water oxidation reaction. *Dalton Transactions* **2015**, *44* (25), 11592−11600.
(35) Lo, Y. L.; Hwang, B. J. In Situ Raman Studies on Cathodically Deposited Nickel Hydroxide Films and Electroless Ni−P Electrodes in 1 M KOH Solution. *Langmuir* **1998**, *14* (4), 944−950.
(36) Trześniewski, B. J.; Diaz-Morales, O.; Vermaas, D. A.; Longo, A.; Bras, W.; Koper, M. T.; Smith, W. A. In situ observation of active oxygen species in Fe-containing Ni-based oxygen evolution catalysts: the effect of pH on electrochemical activity. *J. Am. Chem. Soc.* **2015**, *137* (48), 15112−15121.
(37) Park, S.-A.; Lee, E.-K.; Song, H.; Kim, Y.-T. Bifunctional enhancement of oxygen reduction reaction activity on Ag catalysts due to water activation on LaMnO3 supports in alkaline media. *Sci. Rep.* **2015**, *5*, 13552.
(38) Yuan, L.; Jiang, L.; Liu, J.; Xia, Z.; Wang, S.; Sun, G. Facile synthesis of silver nanoparticles supported on three dimensional graphene oxide/carbon black composite and its application for oxygen reduction reaction. *Electrochim. Acta* **2014**, *135*, 168−174.
(39) Tang, C.; Wang, H.-S.; Wang, H.-F.; Zhang, Q.; Tian, G.-L.; Nie, J.-Q.; Wei, F. Spatially Confined Hybridization of Nanometer-Sized NiFe Hydroxides into Nitrogen-Doped Graphene Frameworks Leading to Superior Oxygen Evolution Reactivity. *Adv. Mater.* **2015**, *27* (30), 4516−4522.
(40) Morgan, D. J. Resolving ruthenium: XPS studies of common ruthenium materials. *Surf. Interface Anal.* **2015**, *47* (11), 1072−1079.
(41) Wang, H.-Y.; Hsu, Y.-Y.; Chen, R.; Chan, T.-S.; Chen, H. M.; Liu, B. Ni3+-Induced Formation of Active NiOOH on the Spinel Ni−Co Oxide Surface for Efficient Oxygen Evolution Reaction. *Adv. Energy Mater.* **2015**, *5* (10), 1500091.
(42) Nayak, S.; Parida, K. M. Dynamics of Charge-Transfer Behavior in a Plasmon-Induced Quasi-Type-II p−n/n−n Dual Heterojunction in Ag@Ag3PO4/g-C3N4/NiFe LDH Nanocomposites for Photocatalytic Cr(VI) Reduction and Phenol Oxidation. *ACS Omega* **2018**, *3* (7), 7324−7343.
(43) Zhang, L.; Wang, S.; Lu, C. Detection of Oxygen Vacancies in Oxides by Defect-Dependent Cataluminescence. *Anal. Chem.* **2015**, *87* (14), 7313−7320.
(44) Tu, Y.; Chen, S.; Li, X.; Gorbaciova, J.; Gillin, W. P.; Krause, S.; Briscoe, J. Control of oxygen vacancies in ZnO nanorods by annealing and their influence on ZnO/PEDOT:PSS diode behaviour. *J. Mater. Chem. C* **2018**, *6* (7), 1815−1821.
(45) El Maliki, H.; Bernède, J. C.; Marsillac, S.; Pinel, J.; Castel, X.; Pouzet, J. Study of the influence of annealing on the properties of CBD-CdS thin films. *Appl. Surf. Sci.* **2003**, *205* (1), 65−79.
(46) Cheng, Z.; Huang, C.; Song, L.; Wang, Y.; Ding, Y.; Xu, J.; Zhang, Y. Electrospinning synthesis of CdIn2O4 nanofibers for ethanol detection. *Sens. Actuators, B* **2015**, *209*, 530−535.
(47) Wang, S.; Nai, J.; Yang, S.; Guo, L. Synthesis of Amorphous Ni−Zn Double Hydroxide Nanocages with Excellent Electrocatalytic Activity toward Oxygen Evolution Reaction. *ChemNanoMat* **2015**, *1* (5), 324−330.
(48) Okamoto, K.; Miyawaki, J.; Nagai, K.; Matsumura, D.; Nojima, A.; Yokoyama, T.; Kondoh, H.; Ohta, T. Structural Study on Highly Oxidized States of a Water Oxidation Complex [RuIII(bpy)2(H2O)]-2(μ-O)4+ by Ruthenium K-Edge X-ray Absorption Fine Structure Spectroscopy. *Inorg. Chem.* **2003**, *42* (26), 8682−8689.
(49) Liu, R.; Wang, Y.; Liu, D.; Zou, Y.; Wang, S. Water-Plasma-Enabled Exfoliation of Ultrathin Layered Double Hydroxide Nanosheets with Multivacancies for Water Oxidation. *Adv. Mater.* **2017**, *29* (30), 1701546.
(50) Guo, J.; Hsu, A.; Chu, D.; Chen, R. Improving oxygen reduction reaction activities on carbon-supported Ag nanoparticles in alkaline solutions. *J. Phys. Chem. C* **2010**, *114* (10), 4324−4330.
(51) Zhou, R.; Zheng, Y.; Jaroniec, M.; Qiao, S.-Z. Determination of the electron transfer number for the oxygen reduction reaction: from theory to experiment. *ACS Catal.* **2016**, *6* (7), 4720−4728.
(52) Gu, X.-K.; Samira, S.; Nikolla, E. Oxygen Sponges for Electrocatalysis: Oxygen Reduction/Evolution on Nonstoichiometric, Mixed Metal Oxides. *Chem. Mater.* **2018**, *30* (9), 2860−2872.
(53) Yang, M.-Q.; Wang, J.; Wu, H.; Ho, G. W. Noble Metal-Free Nanocatalysts with Vacancies for Electrochemical Water Splitting. *Small* **2018**, *14* (15), 1703323.
(54) Subbaraman, R.; Tripkovic, D.; Chang, K.-C.; Strmcnik, D.; Paulikas, A. P.; Hirunsit, P.; Chan, M.; Greeley, J.; Stamenkovic, V.; Markovic, N. M. Trends in activity for the water electrolyser reactions on 3d M(Ni,Co,Fe,Mn) hydr(oxy)oxide catalysts. *Nat. Mater.* **2012**, *11*, 550.
(55) Park, S.-A.; Lee, E.-K.; Song, H.; Kim, Y.-T. Bifunctional enhancement of oxygen reduction reaction activity on Ag catalysts due to water activation on LaMnO3 supports in alkaline media. *Sci. Rep.* **2015**, *5*, 13552.
(56) Cheng, Y.; Dou, S.; Veder, J.-P.; Wang, S.; Saunders, M.; Jiang, S. P. Efficient and Durable Bifunctional Oxygen Catalysts Based on NiFeO@ MnO x Core−Shell Structures for Rechargeable Zn−Air Batteries. *ACS Appl. Mater. Interfaces* **2017**, *9* (9), 8121−8133.
(57) Luo, M.; Cai, Z.; Wang, C.; Bi, Y.; Qian, L.; Hao, Y.; Li, L.; Kuang, Y.; Li, Y.; Lei, X.; Huo, Z.; Liu, W.; Wang, H.; Sun, X.; Duan, X. Phosphorus oxoanion-intercalated layered double hydroxides for high-performance oxygen evolution. *Nano Res.* **2017**, *10* (5), 1732−1739.

DOI: 10.1021/acscatal.8b03092
ACS Catal. 2019, 9, 117−129

(58) Gorlin, Y.; Jaramillo, T. F. A bifunctional nonprecious metal catalyst for oxygen reduction and water oxidation. *J. Am. Chem. Soc.* **2010**, *132* (39), 13612−13614.
(59) Dresp, S.; Luo, F.; Schmack, R.; Kühl, S.; Gliech, M.; Strasser, P. An efficient bifunctional two-component catalyst for oxygen reduction and oxygen evolution in reversible fuel cells, electrolyzers and rechargeable air electrodes. *Energy Environ. Sci.* **2016**, *9* (6), 2020−2024.
(60) Wang, Y.; Zhang, Y.; Liu, Z.; Xie, C.; Feng, S.; Liu, D.; Shao, M.; Wang, S. Layered Double Hydroxide Nanosheets with Multiple Vacancies Obtained by Dry Exfoliation as Highly Efficient Oxygen Evolution Electrocatalysts. *Angew. Chem.* **2017**, *129* (21), 5961−5965.

DOI: 10.1021/acscatal.8b03092
ACS Catal. 2019, 9, 117−129